Six-component seismic land data acquired with geophones and rotation sensors: Wave-mode separation using 6C SVD

Ohad Barak, Priyank Jaiswal, Sjoerd de Ridder, John Giles, Robert Brune, and Shuki Ronen

ABSTRACT

In a three dimensional world there are six degrees of freedom: three linear displacements and three rotations. Current multi-component acquisition systems have geophones or accelerometers that provide the linear motion, and hydrophones that provide the pressure, but without rotations the data are incomplete. We acquired a small seismic survey recording all six components. We deployed three-component geophones and three-component rotation sensors measuring the pitch, roll, and yaw. We measured the pitch independently with closely-spaced geophones to validate the rotation-sensor data. We compare the pitch measured by two independent methods and find that they fit after instrument designature. We then demonstrate that the data provided by rotation sensors have additional value because they can be used in a singular-value decomposition analysis to identify and separate ground roll and body waves.

INTRODUCTION

Rigid bodies in a three dimensional world have six degrees of freedom: three components of linear motion and three components of rotation. The linear motions are recorded by multicomponent geophones, which measure the vertical and the two horizontal components of the particle velocities in the ground. The rotations are the pitch, roll and yaw of the ground, as shown in the following table:

Axis	Displacement		Rotation	
Z	Vertical	v_z	Yaw	r_z
X	Radial	v_x	Roll	r_x
Y	Transverse	v_y	Pitch	r_y

where v_i are particle velocities along the axis, and r_i are rotation rates around the axis.

In marine acquisition, hydrophones record the divergence of the wavefield $P = \nabla \cdot \vec{u}$, where $\vec{u}$ are particle displacements. Rotations are a measurement of the curl

of the wavefield $\vec{r} = \frac{1}{2}(\nabla \times \vec{v})$, and can be recorded by special rotation sensors. If we want to know what the sensor package is doing, and, by inference, which type of wave it is recording, we must measure the three rotations in addition to the three linear components. However, rotations are not recorded by any current commercial multi-component system.

Rotational motion cannot be calculated solely from the 3C particle velocity data acquired by geophones. Figure 1 shows two versions the same trace from the field data of this study. The trace on the left is 3C geophone data, displayed using a "seisball". The seisball represents the motion recorded by the geophones, where up-down motion of the ball is the vertical geophone, left-right motion is the radial geophone, and motion in and out of plane (a change in the seisball size) is the transverse geophone. Unfortunately we are limited in dimensionality on a page, therefore both the time axis and the vertical-motion axis are vertical. The trace on the right displays 3C geophone data *and* 3C rotation data. Observe how the rotations cannot be ascertained from the geophone data, and must be recorded independently.

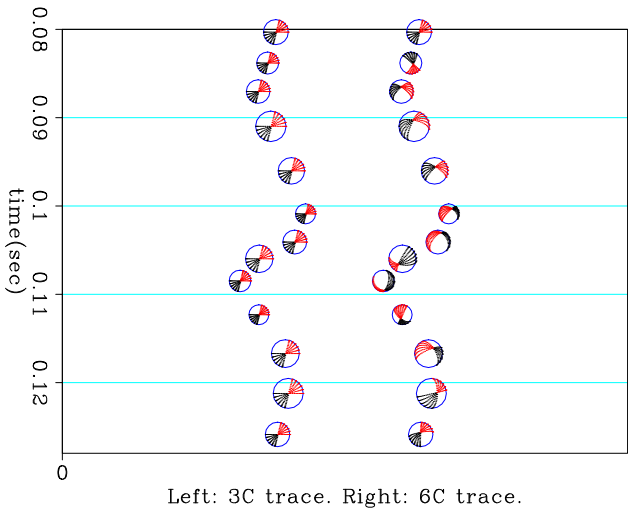

Figure 1: A single trace of the Ponca-City data, shown with seisballs. Left trace is 3C, right trace is 6C. The time and vertical-motion axes are both along the vertical direction. Up-down motion = v_z. Left-right motion = v_x. In-out motion = v_y. The rotations of the ball represent the three rotational components r_z, r_x and r_y. Note that the 6C trace shows rotations that are not seen on the 3C trace. [**ER**]

A seismic sensor that measures three linear motions and three rotations has six components. Lee et al. (2009) review some of the history of rotational seismic acquisition for earthquake seismology. Brokesova and Malek (2010) generated and recorded rotational seismic data using conventional geophones arranged along a circle. Chevron has recently conducted a small land survey that included rotational sensors in order to evaluate the quality and the possible uses for such data. Brune et al. (2012) expand on the added value of 6C data compared to 3C data, including spatial sampling enhancement and shear-wave selectivity. Muyzert et al. (2012) carried out a survey that included rotation sensors, and show how they can effectively double the spatial Nyquist frequency of field data.

In this paper, we show that the rotation sensor's data are additional information. We use six-component polarization analysis on these data to identify and attenuate ground roll.

SURVEY PARAMETERS

The 2D survey took place in a very low relief field near Ponca City, Oklahoma. There were 27 receiver stations. Of these, 18 were single-component vertical geophone stations, 5 were six-component data stations comprising 1 three-component geophone and 1 three-component rotation sensor, and 4 were six-component "cluster" stations, where we had 2 three-component geophones arrayed around a three-component rotation sensor. The receiver stations were spaced 10 m apart. At the six-component cluster stations, the distance between the geophones and the rotation sensor was 30 cm.

The source was an accelerated weight-drop. There were 25 shot stations at 10 m spacing, and these were interspersed inline between the receiver stations. The shortest offset therefore was 5 m, while the longest was 255 m. Consequently, the data have very low fold. Each shot was repeated 5 times at each station, and diversity stacking was applied to the repeated gathers to increase SNR.

DESIGNATURE OF GEOPHONES AND ROTATION SENSORS

A prerequisite for any multicomponent analysis is that all instrument responses must be removed, particularly if the instruments used for each component were different. The instrument response parameters of the geophone components were known. We corrected for the geophone instrument response using the transfer function of a damped harmonic oscillator (Lowrie, 1997; Hons and Stewart, 2006):

$$T(\omega) = \frac{\omega^2}{-\omega^2 + 2i\lambda\omega_0\omega + \omega_0^2}, \tag{1}$$

where natural angular-frequency, ω_0, and the damping ratio, λ, are properties of the suspension spring and electrical circuit. The transfer function was scaled by an overall sensitivity factor, G, with units $\propto V\,\mathrm{m}^{-1}$ s.

The sensitivity of the rotation sensors (of type METR-03) as specified by the manufacturer was $50V\,\mathrm{rad}^{-1}$ s. We were unsure of the phase response of the rotation sensors. To enable further processing however, the instrument response of the rotation sensor had to be removed. We therefore utilized the prediction of elasticity theory for the rotation-rate around the horizontal Y axis for the zero traction boundary condition that exists on the free surface: $r_y = \frac{1}{2}(\nabla \times \vec{v})_y = \partial_x v_z$ (Cochard et al., 2006), i.e. the pitch sensor r_y records the inline horizontal gradient of the vertical component. Therefore the signal calculated by differencing two vertical geophones that are inline and adjacent to the pitch sensor should record the same data as the pitch sensor.

We placed two vertical geophones at a distance of 30 cm upline and downline of

the rotation sensors at receiver stations 19, 23, 27 and 31. Having designatured the geophones, we differenced the signal between these adjacent geophones which were spaced 60 cm apart, thus directly measuring $\partial_x v_z$. We compared the phase spectra of the rotational pitch component r_y and the measured vertical-geophone difference $\partial_x v_z$, and designed a matching filter based on the linear best-fit to the phase difference between them. The bold lines in Figure 2 are the phase differences at the four different cluster stations, and the dashed lines are the frequency-dependent phase corrections applied to the pitch sensors at these stations.

We would prefer not to use closely-spaced geophones to measure rotations in production, since differencing two geophones boosts up noise at the expense of signal. Additionally, each one of the geophones may have a different coupling to the medium. It is necessary to space the geophones used for differencing far enough apart so that the difference signal will be large enough (compared to the boosted noise), and yet they must still be close enough to sample the shortest wavelength without aliasing. In retrospect, we see that a distance of 60 cm between geophones was too close for this particular site, resulting in a loss of geophone-difference signal and probable errors in the measurement of the phase-lag of the rotation sensors for some frequencies. Additionally, in the case of ocean-bottom node acquisition, using multiple geophone differencing is not practical, since all sensors must be encapsulated within the same small package. We only used adjacent geophones in this study to callibrate the rotation sensors.

According to Figure 2, the reliable frequency range we can use to estimate the rotation-sensor's phase by vertical-geophone differencing in this study is $20 - 45$ Hz. Figure 3(a) is the raw receiver gather of the vertical-geophone difference overlain by the pitch sensor. Figure 3(b) is the same gather after correcting for the phase difference between these gathers, and then bandpassing to the frequency range where we have a reliable difference signal. Note the improved match of these components after correcting for the pitch-sensor's phase-lag.

Figure 4(a) is the crosscorrelation of the vertical-geophone difference and the pitch sensor. Note how the maximum energy is not centered at zero time. In Figure 4(b) the same crosscorrelation is shown after applying the matching filter. Both Figures 3(b) and 4(b) show that at station 19, the instrument response of the rotation sensor has been suitably corrected.

SIX COMPONENT FIELD DATA

Figures 5(a)-5(f) are the 6-component receiver gather at station 19, after designature of the geophones and rotation sensors. Coherent energy appears mostly on the v_z, v_x and r_y components (Figures 5(a), 5(b) and 5(f), respectively), which is consistent with the survey's 2D geometry. Three types of arrivals are apparent:

1. Low-wavenumber direct arrivals and what we think are refractions propagating

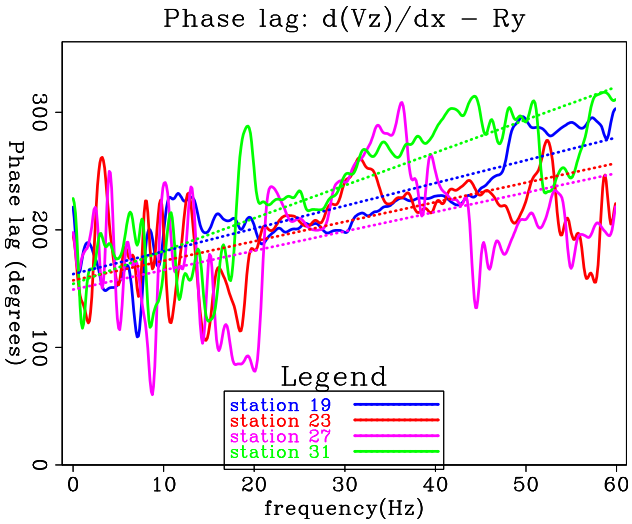

Figure 2: The phase difference between the geophone-difference signal (after designature) and the rotational pitch sensor, plotted over frequency. Solid line: measured difference. Dashed line: best linear fit of difference, which was used to correct the phase of the pitch sensors. [**ER**]

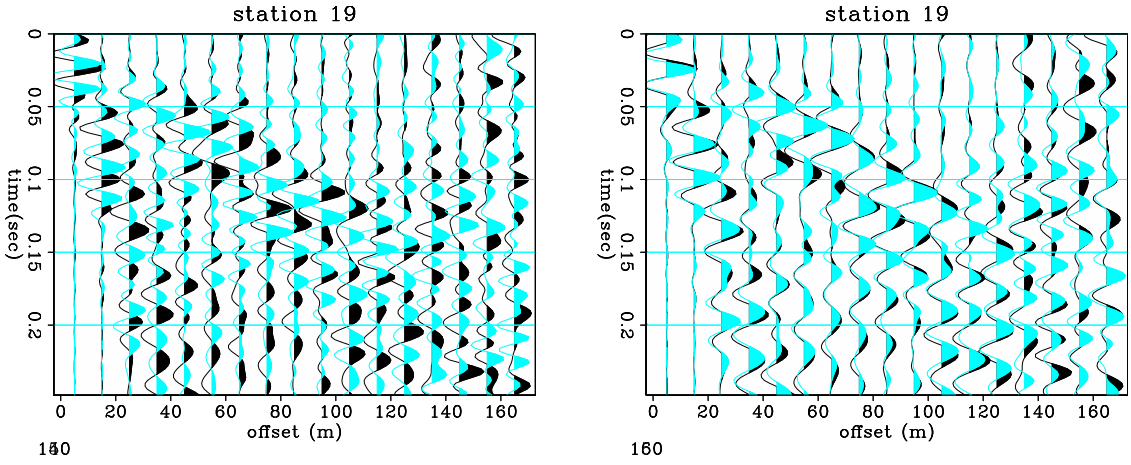

(a) (b)

Figure 3: Comparison of vertical geophone difference signal (black) and rotational pitch component (cyan) for receiver gather at receiver station 19. (a) Raw data. (b) Data after application of matching filter and then filtering between $20 - 45$ Hz. This figure shows that the pitch sensor has indeed been designatured correctly. [**ER**]

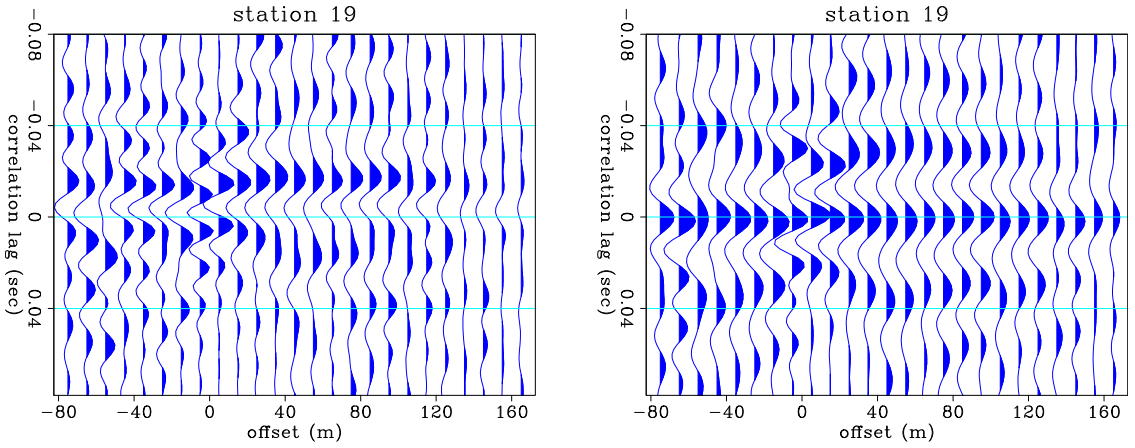

(a) (b)

Figure 4: Crosscorrelation of vertical geophone difference signal and rotational pitch component. (a) Crosscorrelation before matching filter. (b) Crosscorrelation after application of matching filter and then filtering between $20 - 45$ Hz. [**ER**]

at $V \approx 2.4$ km/s, which appear largely on the v_z and v_x components.

2. High-wavenumber Rayleigh waves (ground-roll) propagating at $V \approx 0.9$ km/s. We call this arrival the "fast" ground-roll.

3. A very slow and aliased arrival propagating at $V \approx 0.18$ km/s, which is stronger on the v_z and r_y components. We call this arrival the "slow" ground-roll.

SVD and wave signatures

de Meersman et al. (2006) apply singular-value decomposition (SVD) on three-component geophone data in order to estimate the polarization direction of P-wave arrivals. Similarly, it is possible to apply SVD on 6-component data from a 3C geophone and a 3C rotation sensor. The resulting polarization vectors indicate not only polarization along the linear components, but also polarization along rotational components.

Given a time window of a single 6C trace of length N, we have an $N \times 6$ data matrix where the columns are the components $\mathbf{D} = [v_z(t), v_x(t), v_y(t), r_z(t), r_x(t), r_y(t)]$. SVD is a method for finding the waveform $\mathbf{u}_s$, magnitude σ_s, and polarization $\mathbf{v}_s$ of the signal that is present in the data $\mathbf{D}$. The SVD of the data $\mathbf{D}$ is given by

$$\mathbf{D} = \mathbf{U}\Sigma\mathbf{V}^T, \tag{2}$$

where $\mathbf{D}$ is the product of the Nx6 matrix $\mathbf{U}$, the 6x6 diagonal matrix Σ, and the transpose of the 6x6 matrix $\mathbf{V}$. The unit left and right singular vectors $\mathbf{u}_i$ and $\mathbf{v}_i$

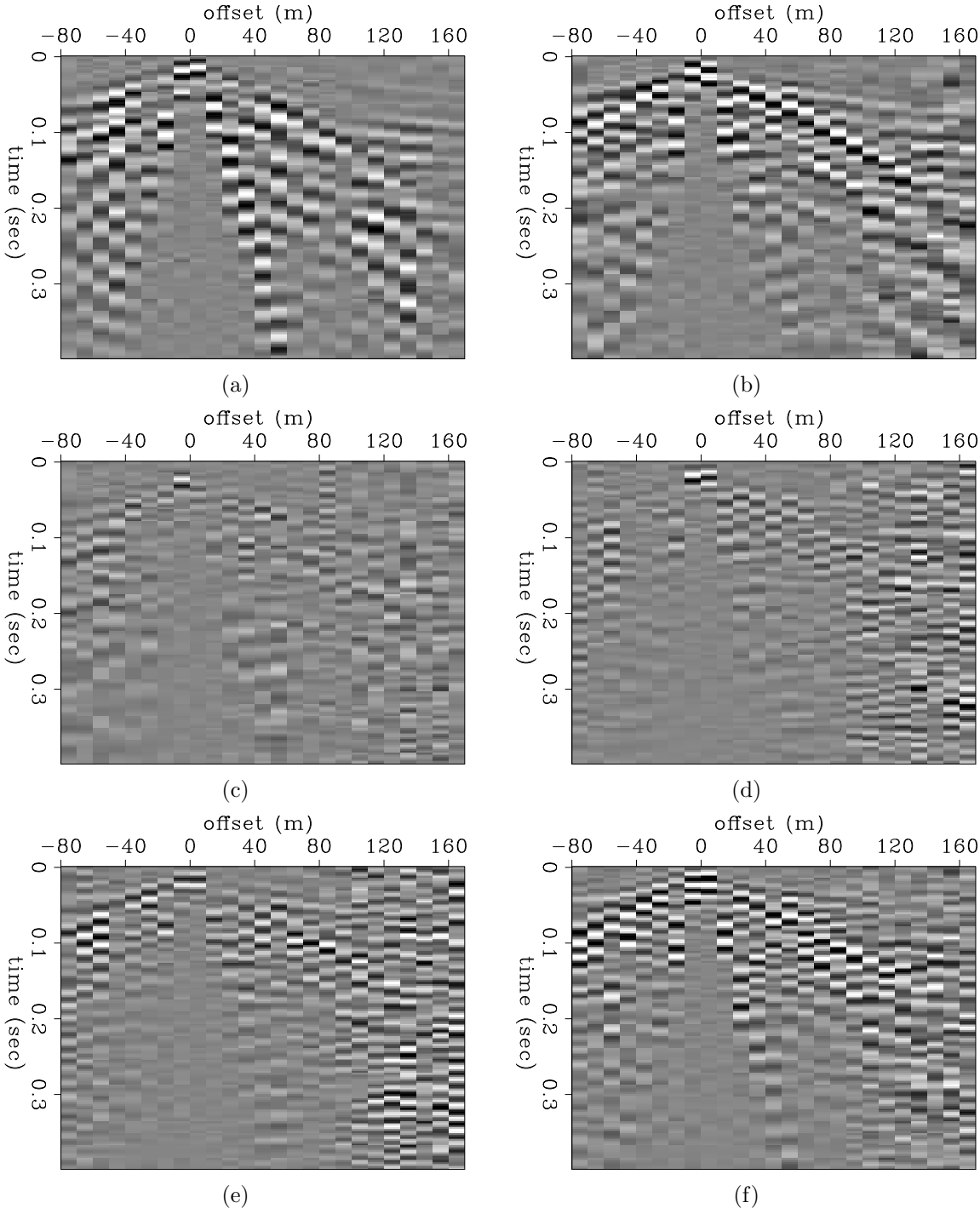

Figure 5: Six-component common-receiver gathers at station 19, with trace balancing applied. (a) Vertical geophone. (b) Radial geophone. (c) Transverse geophone. (d) Yaw sensor (rotation around vertical). (e) Roll sensor (rotation around radial). (f) Pitch sensor (rotation around transverse). Maximum geophone amplitudes are on the order of 3 mm/s, while maximum rotational amplitudes are at 3 mrad/s. The color table in all these figures is in that range. Most of the energy in this 2D survey is on the v_z, v_x and r_y components. [**ER**]

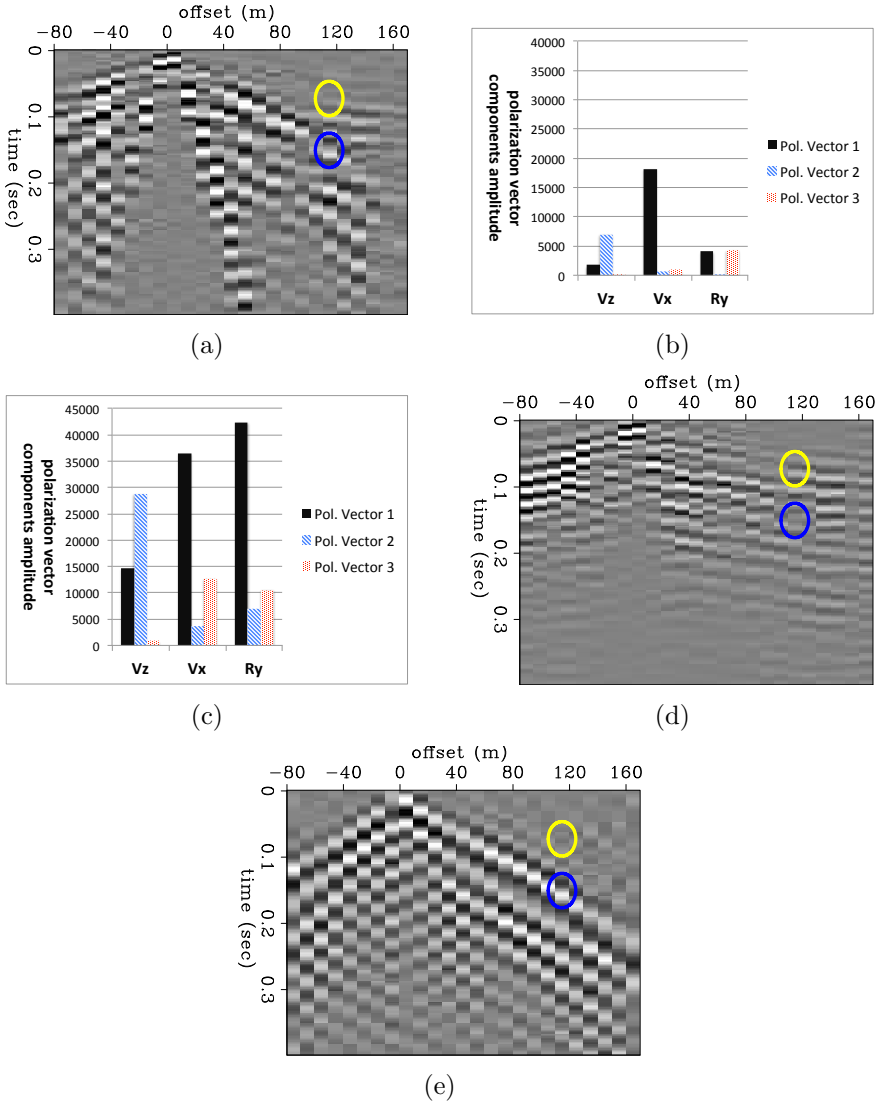

Figure 6: Receiver gather of vertical geophone at station 19, and polarization vectors calculated at trace marked by circles. (a) Vertical geophone. (b) and (c) are the amplitudes of the polarization vectors' components calculated by SVD on the v_z, v_x and r_y components of the single trace at offset=115m; (b) at the time window specified by the yellow circle ($t = [0.07, 0.11]$), (c) at the time window specified by the blue circle ($t = [0.124, 0.164]$). Note how there is a distinct difference in the polarization of the energy in these two time windows. Observe the increased polarization of the 1^{st} polarization vector in the direction of the rotational pitch component for the blue circle, where the Rayleigh-wave is strong. (d) Vertical geophone after F-K filtering to remove high wavenumbers and low frequencies. (e) Vertical geophone after F-K filtering to remove low wavenumbers and high frequencies. [**ER**]

are the six column-vectors of $\mathbf{U}$ and $\mathbf{V}$. The singular values σ_i are the diagonal elements of Σ. They are ordered such that $|\sigma_1|$ is the greatest and $|\sigma_6|$ the smallest. The left and right singular vectors are mutually orthogonal, such that $\mathbf{U}^T\mathbf{U} = \mathbf{I}$ and $\mathbf{V}\mathbf{V}^T = \mathbf{I}$.

The right singular vectors $\mathbf{v}_i$ display the polarization of the data within the particular time window along the six axes. We transpose and multiply the matrix $\mathbf{V}$ by the singular value matrix Σ, to obtain the scaled polarization vectors:

$$\mathbf{S} = \Sigma\mathbf{V}^T. \tag{3}$$

We applied three-component SVD on the vertical, radial and pitch components of the receiver gather shown in Figures 5(a), 5(b) and 5(f) respectively. We did not include the transverse, yaw or roll components as they did not contain significant amounts of coherent energy.

Figures 6(a)-6(c) show how the combination of linear and rotational polarization-vector components provide an indication of the wave type. Figure 6(a) is the raw vertical geophone gather at station 19. We applied trace balancing to the vertical-geophone component, and then used the same balancing weights for the radial-geophone and pitch components (not shown in this figure). SVD of the 3 components was run on two time windows of the trace at offset=115m, which are indicated by the yellow and blue circles. The time-window length was 40 milliseconds.

Figure 6(b) shows the magnitude of the polarization-vector components in directions v_z, v_x and r_y, for the time window indicated by the yellow circle in Figure 6(a). This figure is a display of the elements of matrix $\mathbf{S}$ of equation 3. In black are the components of the first (and largest) polarization vector, the second-largest polarization vector is in blue, and the third-largest in red. There are three polarization vectors since we used only three components for this analysis.

Observe that the 1$^{\text{st}}$ polarization vector is polarized mostly toward the v_x and v_z axes, though the r_y pitch component is present. At this time window, the energy appears to be that of a refraction wave. This can be corroborated by Figure 6(d), which shows the v_z component after F-K filtering removed the high-wavenumber, low-frequency energy. Body waves generate mostly linear particle motion, and should therefore exhibit polarization along the linear components of the 1$^{\text{st}}$ polarization vector.

Figure 6(c) shows the magnitude of the polarization-vector components for v_z, v_x and r_y, for the time window indicated by the blue circle in Figure 6(a). At this time window we have surface-wave energy, as can be seen in Figure 6(e) where F-K filtering removed low-wavenumbers and high-frequencies. Note how the 1$^{\text{st}}$ polarization vector for this time window is polarized mostly on the rotational r_y and linear v_x components. The fundamental mode of surface waves (Rayleigh, Scholte) generates elliptical particle motion, and therefore causes a greater rotational deformation on a finite volume element. We then expect that these waves should be polarized more

toward the rotational components of the 1st polarization vector. Note that the 2nd polarization vector in Figure 6(e) has a dominant v_z component. This is an indication that there is body-wave energy in the data at this time window, but it is obscured by the rotationally-polarized surface wave.

Observe that all wave modes have both rotation and linear motion, owing to the fact that we are recording them on a free surface, where the stress is discontinuous and mode conversions occur. Yet there is still a difference in the relative magnitude of the components of the polarization vectors between the different wave modes. We call the wave modes' appearance on the polarization components a "signature" of the wave mode, by which it may be identified.

FILTERING BY POLARIZATION IN THE SVD SPACE

Our point of view is that all the data which are a result of the seismic experiment is signal, however some of the signal is desired (e.g., reflected body waves) and some is undesired (e.g., surface waves). In a larger context, we wish to be able to differentiate all wave modes from multi-component data according to their polarization attributes. Therefore, the more data attributes we have, the more we are likely to discern among the wave modes. In our study, these additional attributes come from rotation data. Both displacement and rotation are a result of the deformation caused by wavefronts incident on the recording surface. The combination of linear displacements and rotational data components, i.e. their "signature", maps to the wave modes generating the deformation.

The method we employ here is to estimate the direction of the 1st polarization vector from a portion of the data that contains the undesired signal. We use this vector as a "template" for the polarization of that undesired signal. We search for this template by applying SVD to sliding time windows along the data, and calculating the angular difference θ_{diff} between the 1st polarization vector at that time window $\vec{V}(t)$ and the 1st template polarization vector $\vec{V}_{\text{temp}}$:

$$\theta_{\text{diff}}(t) = \cos^{-1}\left(\frac{\vec{V}(t)\cdot\vec{V}_{\text{temp}}}{\left|\vec{V}(t)\right|\left|\vec{V}_{\text{temp}}\right|}\right). \tag{4}$$

We design a weighting function that damps the 1st singular value in the Σ matrix from equation 2 based on θ_{diff}:

$$W(t) = 1 - \cos^2\left(\frac{\theta_{\text{diff}}(t)}{\theta_{\max}}\right). \tag{5}$$

We apply the weighting to the 1st singular value in each time window, and then recompose the data using equation 2. Effectively, we damp the energy of the 1st

singular vector based on how similar it is to the 1st polarization vector of the template signal. The two independent variables that must be defined are the time-window length, and the angular difference threshold $\theta_{\max}$.

There are two assumptions that must be met for this damping method to succeed in attenuating the undesired signal:

1. There needs to be a significant difference between the direction of the polarization of the undesired signal vs. that of the desired signal. Ideally, they would be orthogonal.
2. The undesired signal's energy must dominate that of the desired signal. Otherwise, the 1st polarization vector will point in an intermediate direction between these two signals, and a damping of this polarization vector would result in a loss of both signals.

The polarization strength of a multicomponent signal is a measure of how dominant the 1st polarization vector is relative to the other vectors, and can be estimated by (Vidale, 1986):

$$P_s = 1 - \frac{\sum_{i=2}^{n} \sigma_i}{\sigma_1}, \tag{6}$$

where σ_i are the singular values pertaining to polarization vectors 2 to n, and σ_1 is the singular value of the 1st polarization vector. P_s is near 1 if the signal is completely polarized in the direction of the 1st polarization vector, but is near 0 if the largest component of polarization is only as big as the rest combined. For 3C geophone data, $P_s = 1$ means a linearly polarized signal. The interpretation for a combination of linear and rotational components is more complicated.

We use the polarization strength to gauge where on the seismogram we would expect that a damping of the 1st polarization vector by its similarity to a particular polarization signature from the data would result in an actual attenuation of energy. Figure 7 shows the polarization strength P_s calculated for station 19, together with the vertical geophone component at that station. There is a high polarization strength underlying the fast ground-roll arrival between $t = 0.05 - 0.13$ sec at offsets $x = 35 - 95$ m. It is also high for the very slow ground-roll that begins at zero-offset and continues till offset $x = 55$ m at the end of the section. However, for most this section there is no dominance of a particular polarization direction. Since we expect that for distinct strong signals there will be a dominant polarization direction, we deduce that this data has low SNR. Therefore we may only expect limited attenuation of undesired arrivals such as the surface wave, by such damping of the 1st polarization vector on this dataset.

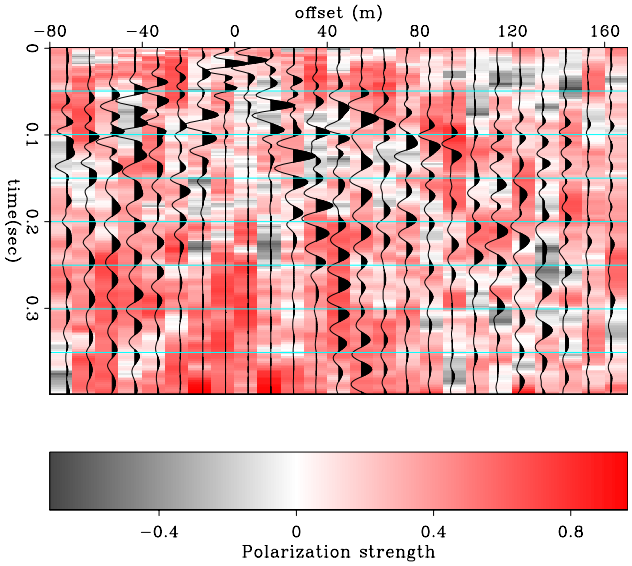

Figure 7: Vertical component at station 19 overlaying the polarization strength. Values closer to 1 (red) indicate that the 1st polarization vector is significantly larger than all other polarization vectors, and we can therefore expect that in such regions the damping of the 1st polarization vector will result in a significant removal of energy polarized in that direction. [**ER**]

Estimating signature of undesired signals

Our undesired signal in this case are the two surface waves which we called "fast" and "slow" ground-roll. In order to estimate their signature, we applied a linear moveout with velocity $v = 820\,\mathrm{m/s}$ for the fast ground roll, and with $v = 180\,\mathrm{m/s}$ for the slow ground-roll. We then stacked each one of these sections. We applied SVD to the time window containing the stacked ground roll energy, and selected the 1st polarization vector as a template. Afterwards, we applied the methodology detailed above to damp the 1st polarization vector of the data along running time windows. We used a 40 ms time window length, and $\theta_{\max} = 20^o$.

Figures 8(a), 8(c) and 8(e) show the vertical, radial and pitch components respectively, after filtering using the slow ground-roll signature as a template. The underlying color indicates the damping weight, where white indicates maximal damping. Black wiggles are the data before filtering, and cyan wiggles are after filtering.

The template signature was estimated on the slow ground roll, however we can see that other portions of the data have polarization attributes similar to the slow ground-roll signal. Most of the energy that is attenuated is on the vertical component.

Figures 8(b), 8(d) and 8(f) show the vertical, radial and pitch components respectively, after filtering using the fast ground-roll signature as a template. This filtering was applied to the results of filtering the slow ground-roll. Note how now the attenuation concentrates on the fast ground-roll, but does leak to include some of the refractions appearing at offsets $x = 80_m - 160_m$ at around $t = 0.1_s$. This indicates that the polarization of the undesired signal, in this case the ground-roll, is not orthogonal to the polarization of the desired signal. Most of the attenuation though is from the horizontal component, and the fast ground-roll is mostly removed.

Figures 9(a), 9(c) and 9(e) again show the vertical, radial and pitch components

before filtering, but on a greyscale. Figures 9(b), 9(d) and 9(f) are the same components after filtering.

The low SNR ratio of these data make it difficult to gauge exacly how much of the desired signal is removed along with the attenuation of the undesired signal. However, comparing Figures 9(a) and 9(b) we see that a large proportion of the ground-roll has indeed been attenuated from the vertical component, without a great adverse effect on the desired signal, i.e., the refractions apparent on the top right section.

Comparing the radial component's attenuation in Figures 9(c) and 9(d), we see that along with the undesired ground roll we seem to have eliminated a large part of the desired signal as well. We attribute this to a similarity in the direction of the 1^{st} polarization vector of this signal to the ground roll's signature. It is very difficult to discern any coherent signal on the pitch component, other than the ground-roll itself. In general, we have noticed that the SNR of the rotation sensors is not as good as that of the geophones, so this is not surprising.

DISCUSSION: FROM COMPONENTS TO WAVE MODES

Particle displacements and rotations are data components. P-waves, shear waves and surface waves are wave modes. Conventional state of the art multicomponent data processing assumes that P-waves register on the vertical displacement components, while shear waves register on the horizontal components. However, in principle what we should record are not displacements, which are characteristic to all wave modes, but strains, which are a better differentiator between wave modes than particle motion. An example of a sensor that records P-wave strains is a hydrophone. A rotation sensor effectively records the anti-symmetric strains, which are a characteristic of shear waves and surface waves.

We do not want to see waves that appear as shear waves or surface waves on the vertical displacement component. We call this kind of energy "shear-induced" or "Vz" noise (Craft and Paffenholz, 2007), and usually attempt to attenuate it using local dip filtering. A problem with such noise attenuation methods is that they depend on adequate spatial sampling of all wave modes, and they may harm the data if they have temporal and spatial characteristics similar to the noise. Rotation data can aid us in finding alternate methods of identifying the wave modes responsible for generating the shear-induced noise, and also in separating them from the data that carry information about the subsurface.

The identification of wave modes using polarization analysis of single traces is similar to the approach taken by Diallo et al. (2006), where polarization analysis in the complex-wavelet domain is used to attenuate surface waves without the use of local wavenumbers. We intend to investigate complex wavelet analysis for 6C data as well, since it can provide a frequency resolution of the data over time. Different wave modes may have different frequency characteristics which we can exploit for separation. SVD of 6C data can make methods like de Meersman et al. (2006) more robust, especially

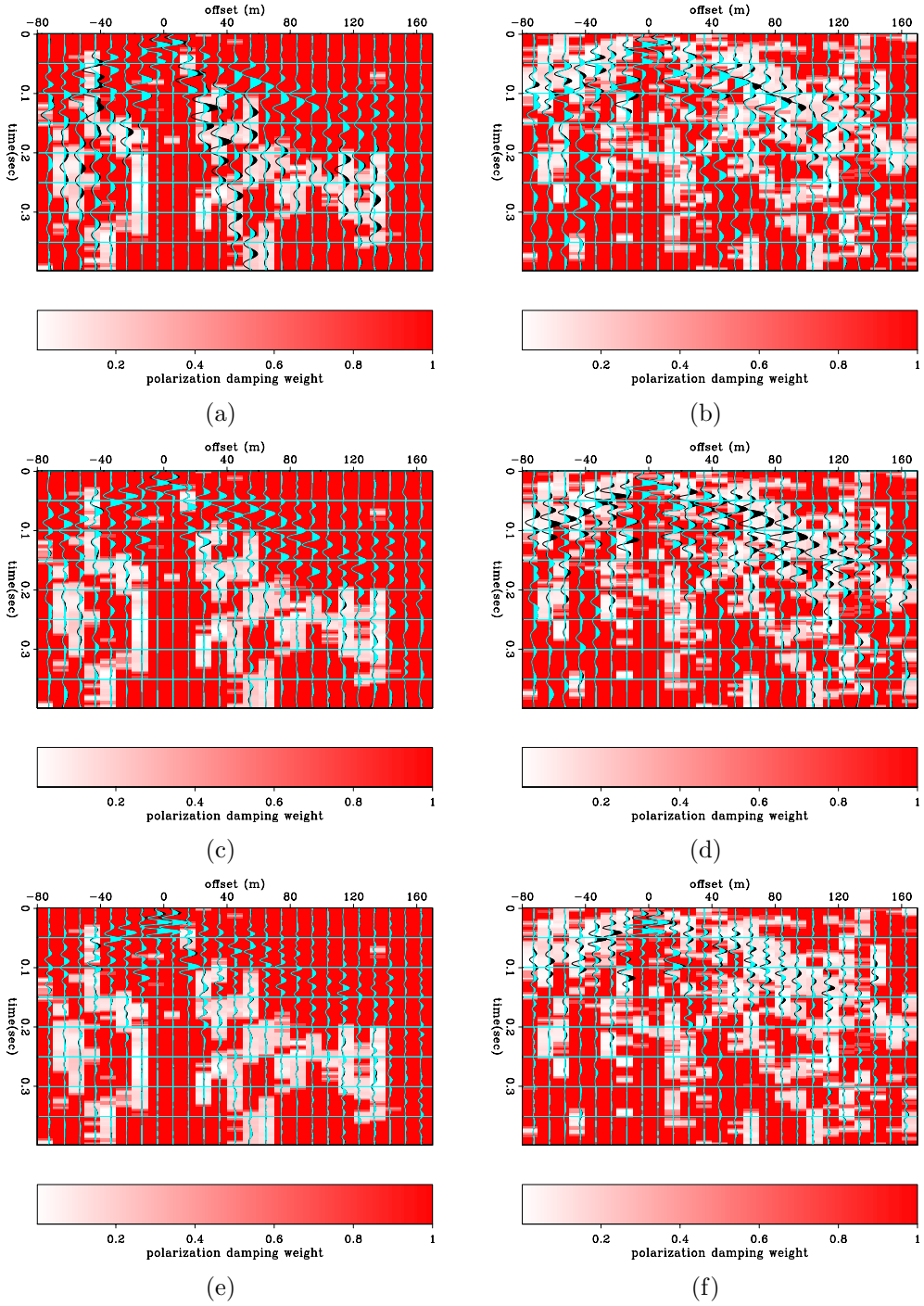

Figure 8: Data components at station 19, before filtering (black) and after filtering (cyan) by damping of the 1st polarization vector according to its similarity to the stacked ground-roll signals. The data overlays the damping weight. (a) Vertical component, damping slow ground-roll. (b) Vertical component, damping fast ground-roll. (c) Radial component, damping slow ground-roll. (d) Radial component, damping fast ground-roll. (e) Pitch component, damping slow ground-roll. (f) Pitch component, damping fast ground-roll. Note how the damping is restricted to the region where the polarization is similar to the SVD signature chosen. [**ER**]

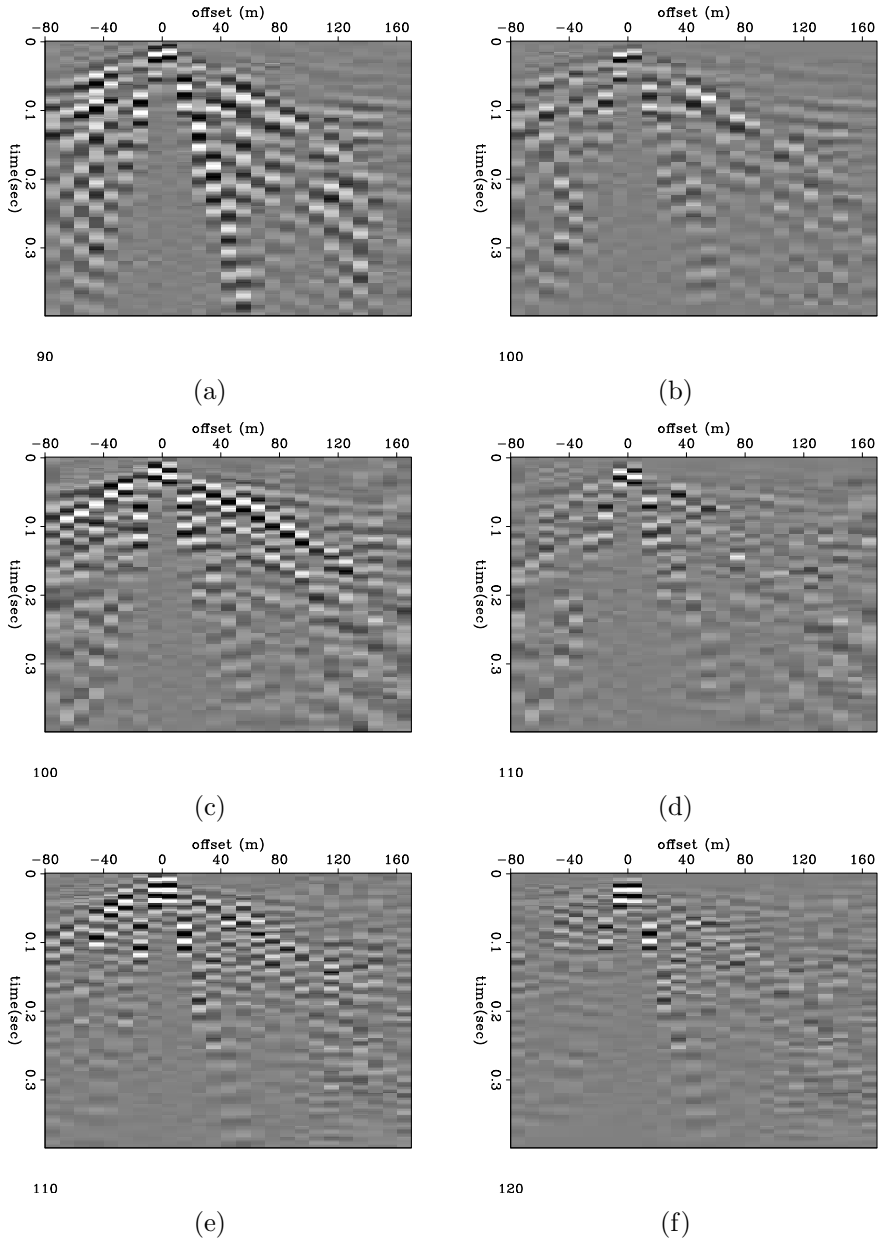

Figure 9: Data components at station 19, before and after filtering by signatures. (a) Vertical component before filter. (b) Vertical component after filter. (c) Radial component before filter (d) Radial component after filter. (e) Pitch component before filter. (f) Pitch component after filter. The slow and fast ground roll signals are attenuated on the vertical component, apparently without much loss of other signals. However for the radial component there seems to be a significant loss of signal together with the attenuation of the ground roll. [**ER**]

for non-radial scattering. We believe that rotation data can augment such methods by introducing additional data about the strains, which are different for different wave modes.

SUMMARY

We conducted a field experiment and validated that the measurements of rotation sensors agree with those from closely-spaced geophones. We observe that rotation data helps identify different wave modes by providing independent information that in practice cannot be derived from the geophones without the rotation sensors. We designed a filter that attenuates the main polarization of the data along time windows, according to the data's similarity to a template polarization signature taken from the undesired portion of the data. We observe limited success of this method on our field dataset. We speculate that a dataset with better SNR may yield better separation results. To observe the effect of such a wave-mode separation on imaging, however, we would require much higher-fold, long-offset 3D 6-component data.

ACKNOWLEDGEMENTS

We wish to thank the Mcgee-Levorsen research grant program, the Boone-Pickens School of Geology, and Dan Braden and Damon Dawes from Seismic Source Co. for their extensive support, expertise and practical knowledge on running surveys in the field. Thanks also to Everhard Muyzert for fruitful discussions on this project.

REFERENCES

Brokesova, J. and J. Malek, 2010: 2nd IWGoRS Workshop in Prague.

Brune, R., D. Aldridge, M. van der Baan, J. Gaiser, and E. Muyzert, 2012, Theta-data: Introduction to rotational seismology and its potential uses: 82nd SEG Conference and Exhibition.

Cochard, A., H. Igel, B. Schuberth, W. Suryanto, A. Velikoseltsev, U. Schreiber, J. Wasserman, F. Scherbaum, and D. Vollmer, 2006, Rotational motions in seismology: Theory, observations, simulation: Earthquake Source Asymmetry, Structural Media and Rotation Effects, 391–411.

Craft, K. and J. Paffenholz, 2007, Geophone noise attenuation and wavefield separation using a multidimensional decomposition technique: SEG Technical Program Expanded Abstracts, 2630–2634.

de Meersman, K., M. van der Baan, and J. Kendall, 2006, Signal extraction and automated polarization analysis of multicomponent array data: Bulletin of the Seismological Society of America, **96**, 2415–2430.

Diallo, M., M. Kulesh, M. Holschneider, F. Scherbaum, and F. Adler, 2006, Characterization of polarization attributes of seismic waves using continuous wavelet transforms: Geophysics, **71**, V67–V77.

Hons, M. and R. R. Stewart, 2006, Transfer functions of geophones and accelerometers and their effects on frequency content and wavelets: CREWES research report, **18**.

Lee, W. H. K., H. Igel, and M. D. Trifunac, 2009, Recent advances in rotational seismology: Seismological Research Letters, **3**, 479–490.

Lowrie, W., 1997, Fundamentals of geophysics, 2nd ed.: Cambridge University Press.

Muyzert, E., A. Kashubin, E. Kragh, and P. Edme, 2012, Land seismic data acquisition using rotation sensors: 74th EAGE Conference and Exhibition.

Vidale, J. E., 1986, Complex polarization analysis of particle motion: Bulletin of the Seismological society of America, **76**, 1393–1405.